The Planetary Science Journal, 2:36 (9pp), 2021 February https://doi.org/10.3847/PSJ/abd63b

Standing on Apollo's Shoulders: A Microseismometer for the Moon

Ceri Nunn[1], William T. Pike[2], Ian M. Standley[3], Simon B. Calcutt[4], Sharon Kedar[1], and Mark P. Panning[1]
[1] Jet Propulsion Laboratory, California Institute of Technology Pasadena, CA, USA; ceri.nunn@jpl.nasa.gov
[2] Department of Electrical and Electronic Engineering, Imperial College London, UK
[3] Kinemetrics, Pasadena, CA, USA
[4] Department of Physics, University of Oxford, UK
Received 2020 August 7; revised 2020 December 9; accepted 2020 December 10; published 2021 February 24

Abstract

Seismometers deployed on the Moon by the Apollo astronauts from 1969 to 1972 detected moonquakes and impacts, and added to our understanding of the lunar interior. Several lunar missions are currently being planned, including the Commercial Lunar Payload Services (CLPS), the Lunar Geophysical Network, and the astronaut program Artemis. We propose a microseismometer for the Moon: the Silicon Seismic Package (SSP). The SSP's sensors are etched in silicon, and are predicted to have a noise floor below 2×10^{-10} (m s^{-2})/$\sqrt{\text{Hz}}$ between 0.3 and 3 Hz (similar to the Apollo instruments between 0.3 and 0.5 Hz, and better than Apollo above 0.5 Hz). The SSP will measure horizontal and vertical motion with the three sensors in a triaxial configuration. The instrument is robust to high shock and vibration and has an operational range from −80°C to +60°C, allowing deployment under harsh conditions. The first-generation version of this sensor, the SEIS-SP, was deployed on Mars in 2018 as part of the InSight mission's seismic package. We will reconfigure the seismometer for the lower gravity of the Moon. We estimate that a single SSP instrument operating for one year would detect around 74 events above a signal-to-noise ratio of 2.5, as well as an additional 500+ above the noise floor. A mission lasting from lunar dawn until dusk, carried on a CLPS lander, could test the instrument in situ, and provide invaluable information for an extensive future network.

Unified Astronomy Thesaurus concepts: Lunar seismology (973); Lunar interior (959)

1. Introduction

From 1969 to 1972, Apollo astronauts deployed seismic experiments on the Moon. These experiments led to many new insights into the structure of the Moon (see Garcia et al. 2019 for a recent review). Now, half a century after the first Moon landings, several lunar missions are being planned. These include various Commercial Lunar Payload Services missions (CLPS), the Lunar Geophysical Network (LGN), and the Artemis program. We propose a Silicon Seismic Package (SSP) microseismometer for the Moon to begin a new era of lunar discovery.

CLPS is a NASA program to use commercial companies to deliver payloads to the surface of the Moon (NASA 2019). NASA expects that the competitive nature of the program will reduce the cost of lunar exploration. NASA has already selected twenty-four payloads and experiments (NASA 2019; Richardson 2019), and plan to make future selections. Second, the LGN is a mission currently in formulation for NASA's New Frontiers 5 Announcement of Opportunity (Neal et al. 2020a). The network would include three to four sites containing geophysical instruments, including seismometers (Neal et al. 2020b). Third, the Artemis mission is underway (NASA 2019). In Greek mythology, Artemis was Apollo's twin. Artemis will build upon the success of Apollo and would see humans return to the Moon as early as 2024. Finally, we are pursuing a mission concept where seismometers are delivered to the Moon by penetrators. Penetrators are bullet-shaped vehicles designed to penetrate a surface, and embed instruments beneath the ground. The SSP microseismometer is suitable for these different missions. Using the CLPS program would have the advantage of proving the technology on an earlier, smaller mission. The LGN would be a seismic network with several nodes, which has many benefits over a single station. It has better coverage and allows for more accurate locations of the seismic events. By using the different mission classes (and developing instruments that can operate for several years), we can increase scientific return and cover more regions of the Moon.

The first-generation version of the SSP, the SEIS-SP, was deployed on Mars in 2018 as part of the InSight missions seismic package (Pike et al. 2013; Lognonné et al. 2019). The SEIS-SP uses Micro-Electro-Mechanical Systems (MEMS) sensors. The SSP has potential for operation on the Moon (Pike et al. 2016a) and other planetary bodies (Pike et al. 2016b). We outline changes to the sensor which are required for it to operate in a lunar environment. Fortuitously, these changes will reduce the noise floor compared with a similar instrument operating on either Earth or Mars.

A critical question is whether the instrument is likely to detect sufficient moonquakes. Commercial missions may only operate for a single lunar day (approximately two weeks in Earth time). We can use the seismic events and seismic noise recorded by the Apollo seismometers to estimate the threshold of detection and the number of events.

2. The InSight SEIS-SP Sensor

InSight's SEIS-SP microseismometer, deployed in 2018, consists of a set of three sensors (Pike et al. 2013; Section 5.2 in Lognonné et al. 2019). The sensors are small and lightweight, and are micromachined from single-crystal silicon (with a 25 mm die size), by deep reactive-ion etching to

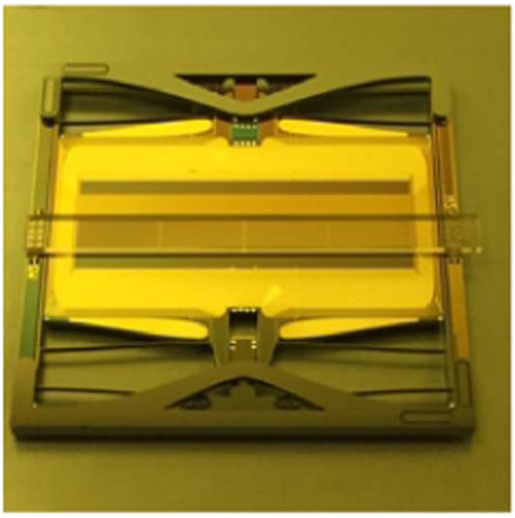

Figure 1. Front view of InSight's SEIS-SP vertical-axis microseismometer, showing the glass strip of the displacement transducer, the solder-ball shock protection and the strengthening buttresses (the die is 25 × 25 mm). The Lunar SSP is a second-generation version of this sensor. (© Imperial College London.)

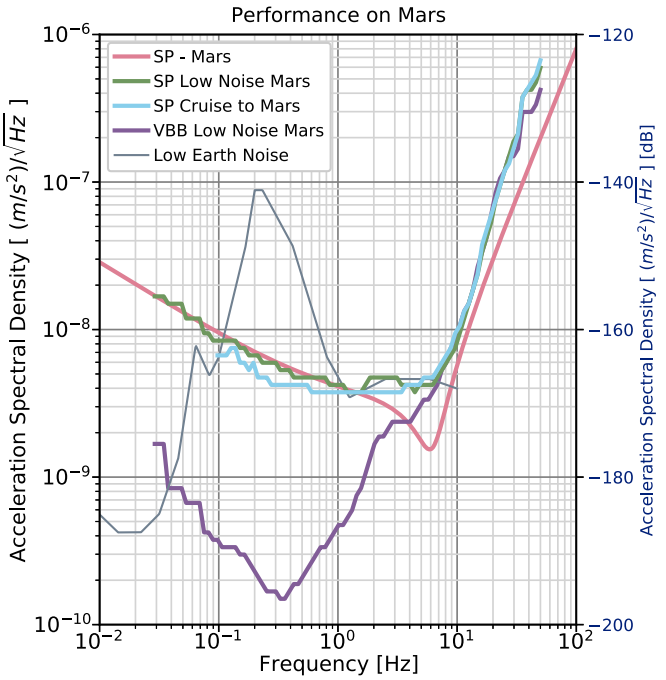

Figure 2. Noise recorded on the SEIS-SP (green line) and SEIS-VBB (purple line) during a quiet period shortly after ground deployment on Mars, and on the SEIS-SP (blue line) during a quiet period during the cruise to Mars. The pink line shows the theoretical noise floor of the SEIS-SP instrument.

produce a suspension and proof mass (Figure 1). Imperial College, the University of Oxford, and Kinemetrics developed the sensors. For more information about the instrument construction, see Pike et al. (2018). The three sensors measure the three components of translational motion. The combined package for InSight had a total mass of 635 g for the three sensor heads, the electronics board and associated connectors and cabling (Pike et al. 2016b). As it required no leveling, the two horizontal sensors were operational during the cruise to Mars, and all three sensors were operational on the lander's deck before full deployment on the ground. Figure 2 shows spectra from quiet periods during the cruise to Mars and after ground deployment. Figure 2 shows that the SP instrument is approximately one-to-two times less sensitive at 3 Hz and ten times less sensitive at 1 Hz than the SEIS-VBB (the main seismometer operating on Mars).

3. A Broadband SSP Microseismometer for the Moon

We are designing the SSP, a second-generation version of the SEIS-SP. Through making the necessary changes required to make the instrument work on the Moon, we can reduce several of the noise sources and lower the overall noise floor (Figure 3). The suspension, which has to accommodate the initial displacement under gravity, will be less stiff to compensate for the lower lunar gravity compared with Earth or Mars. Using a weaker spring (and the same mass) will result in a longer resonance period for the instrument, reducing the noise from thermodynamic sources and from the capacitive displacement transducer (DT). The performance of InSight's SEIS-SP sensor is limited by the thermodynamic noise floor from gas damping within the package (Pike et al. 2016a). It will be possible to operate the seismometer on the Moon under ambient pressure, without additional complications relating to evacuating a chamber, which will further reduce the thermodynamic noise floor. In this section we describe the noise sources for the seismometer, and the improvements we can make (see plot_seismometer_noise.ipynb in the GitHub repository for the parameters and equations used in our estimates).

A combination of the feedback and the suspension provides the restoring force to keep the proof mass stationary. It is difficult to provide a large restoring force for the mass from feedback alone without injecting substantial noise from the feedback electronics. Instead, the engineers design the suspension to counteract the dominant, gravitational force acting on the sensor. The suspension accommodates an initial displacement under gravity of g_x/ω^2, where g_x is the component of gravity along the sensing axis x and ω is the suspension resonance. Additionally, using a triaxial geometry reduces g_x. A triaxial (or Galperin) geometry uses three orthogonal sensors which are separated by 120° azimuth and tilted 55.74° from the vertical. The orientation can be visualized as a cube balanced on one corner. The microseismometer is designed to operate in the reduced gravity of the Moon ($g_M = 1.62\,\mathrm{m\,s^{-2}}$). Therefore, with a triaxial configuration, g_x is $1.62 * \sin(35.26) = 0.935\ \mathrm{m\,s^{-2}}$.

The microseismometer (Figure 1) operates as a force-feedback accelerometer. The displacement of the mass on a spring is detected, and the feedback force required to keep the mass stable provides a velocity output from the feedback electronics. We will lower the resonant frequency from 6 Hz (for Mars) to 2 Hz (for the Moon). A 2 Hz resonance suspension therefore will need to accommodate $g_x/(2 * \pi * f_0)^2 = 6$ mm displacement. The tilt tolerance in the design is 15°.

For testing within the Earth's gravity field, we can tilt the mounted sensors into a new orientation which is further from the vertical. To find the correct angle on Earth, we can make the force acting on the sensor on the Moon and Earth equivalent:

$$mg_E \sin\Theta_E = mg_M \sin\Theta_M,$$

where m is mass, g_E and g_M are Earth and Moon's gravity, and Θ_E and Θ_M are the angles from the horizontal on the Earth and

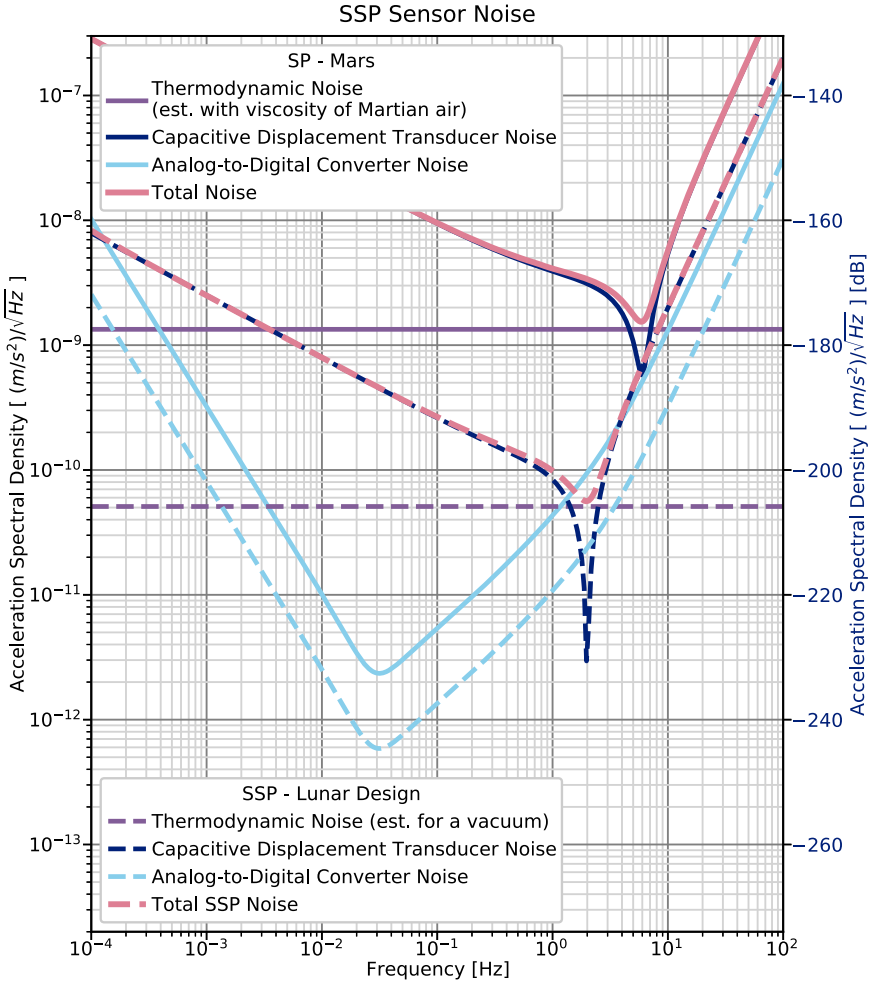

Figure 3. Predicted noise floor for the SSP microseismometer for the Moon (dashed pink line) and current noise floor for the instrument operating on Mars (solid pink line). The estimated thermodynamic noise is significantly improved between Mars (solid purple line) and the Moon (dashed purple line). The capacitive displacement transducer noise is sharply peaked at the resonant frequencies for the instrument on Mars (solid dark-blue line) and the Moon (dashed dark-blue line). The noise floor for the analog-to-digital converter is lower for the lunar design (dashed light-blue line), than for the instrument on Mars (solid light-blue line), as we can increase the output gain by a factor of four owing to lower background noise on the Moon. The reduced gravitational force on the Moon allows us to use a weaker spring. For the same mass, this gives a longer period, which results in lower thermodynamic noise.

Moon. As we are using a triaxial geometry, $\Theta_M = 35.26°$, as $\sin\Theta = 1/\sqrt{3}$. Therefore, $\Theta_E = 5.5°$ and the angle from the vertical is 84.5°.

The design balances the noise power injected by each source to minimize the noise floor in the required bandwidth. Figure 3 shows the expected improvements for the each of the noise sources for the SEIS-SP instrument operating on the Moon. There are three main sources of noise: the thermodynamic noise, the capacitive DT noise, and the analog-to-digital converter (ADC) noise. We minimize the power of each noise source and maximize the amplitude of the previous gain stage in the signal pathway. The suspension takes the acceleration of the proof mass as its input. The thermodynamic fluctuation-dissipation theorem governs the noise injection (Gabrielson 1993). The suspension gain is the second-order transfer function of the damped spring-mass system. Minimization of the noise requires the lowest damping, and the largest mass achievable within the resource constraints of the sensor.

The next subsystem in the noise model is the capacitive DT. The DT determines the position of the mass from the overlap between the two facing arrays of electrodes. One set is mounted on the mass, and the other is fixed across the frame of the suspension. The displacement is measured using a synchronous demodulation technique where a differential sinusoidal drive is applied to one set of plates and the resulting signal appearing on the pick-up plate is synchronously demodulated resulting in a signal proportional to the displacement of the proof mass.

The DT is thought to be contaminated with two noise sources. The first is due to the buffer amplifier and the thermal noise of the DT's preamplifier. The second source is the flicker contribution of the first preamplifier. Thermal noise (also known as Johnson noise) occurs because the atoms of a solid state conductor vibrate and bump into the conducting electrons. This imposes a new, random motion on those conductors which generates noise. Flicker noise (also known as $1/f$ noise) occurs in almost all electronic devices, and it has a variety of different causes, although these are usually related to the flow of direct current, as resistance fluctuations are transformed to voltage or current fluctuations by Ohm's law. It dominates at low frequencies.

The DT input-referred noise in acceleration is shaped by the transfer function of the suspension. It rises in amplitude as $1/f^{1/2}$ below the resonant frequency, and as f^2 above the resonant frequency. The $1/f$ flicker noise is believed to be

introduced at the demodulation stage. We estimate that the lowest point of the DT curve can be reduced by a factor of four, due to a combination of improved DT geometry, and preamplifier. We can decrease the spacing between the DT electrodes because the sensor will be operating in a near vacuum, and therefore, the damping, and hence the suspension noise, will not be increased by reducing this spacing. Halving the spacing will halve the DT noise. We can further minimize the DT noise contribution with a suitable choice of preamplifier, which reduces both the internal voltage noise and current noise contribution from the external resistive components by a factor of two. The preamplifier should have the lowest possible capacitance to reduce the attenuation of the DT gain. We use a modulated drive frequency for the DT, which is well above the corner frequency at which flicker noise rises above the Johnson noise. We choose $15\,\mathrm{nV}/(\sqrt{\mathrm{Hz}})$ for the combined preamplifier noise contributions, this allows either the selection of a relatively low power operational amplifier with less than $10\,\mathrm{nV}/(\sqrt{\mathrm{Hz}})$ noise, or a discrete JFET amplifier design which can offer improved noise of $\sim$5–6 $\mathrm{nV}/(\sqrt{\mathrm{Hz}})$ at the cost of higher power and circuit complexity. A suitable choice of preamplifier gain ensures that noise contributions from the feedback electronics are negligible.

The final noise injection is from the ADC. We set the voltage level of the least-significant bit to be below the DT noise. The output gain is increased by a factor of four, compared with the Mars implementation, which reflects the lower background noise expected on the Moon relative to Mars. The maximum dynamic range is dependent on the number of bits of the ADC (which is 24 bits).

The instrument is demonstrated to be robust to shock and vibration, and has a large operational temperature range. Survival of the proof mass suspension for the InSight SEIS-SP was demonstrated for in-plane vibration levels up to 32 g_0 rms (Lognonné et al. 2019).[5] During tests on a dynamic shaker table, Hopf et al. (2010) found that the silicon crystal in the instrument suspension could sustain a maximum of 75 g_0 in-plane and 35 g_0 out-of-plane acceleration before damage began to occur. For additional shock protection, Hopf et al. (2010) added sublimants such as paradichlorobenzene. The sensors survived shock loads of 15,000 g_0 without incurring damage. This shock tolerance has only been demonstrated for the sensors, not for the entire microseismometer.

The surface temperature of the Moon ranges from 127°C to −173°C, or as low as −238°C in the permanently shadowed regions. The SEIS-SP was tested over an extended temperature range in a thermal test chamber, and demonstrated operation from −80°C to +60°C (Pike et al. 2018). Pike et al. (2016b) showed that the sensor can move freely while immersed in liquid nitrogen (−196°C). The mounting hardware currently restricts lowering the operating temperature. We are changing the materials to better match the silicon thermal expansion coefficient and re-aligning the fasteners to avoid introducing any stress while mounting the magnetic circuit around the sensor. At the upper end of the temperature range, the SEIS-SP sensors are known to survive up to 110°C (as they were baked to meet planetary protection rules). The next step is to test the upper limit of temperature operation. Additionally, we are working on integrating the seismic package with a thermal switch, to protect the instruments from prolonged temperature extremes without the need for active control systems (Clark et al. 2020).

The overall mass of the instrument will be similar to the 0.635 kg mass of the SEIS-SP (Pike et al. 2016b). This mass includes the packaged sensor heads, the electronics board and associated connectors and cabling. The power requirement is 360 mW, which includes power to each of the sensors (Pike et al. 2016a).

In summary, reducing the resonant frequency and damping in the new SSP design reduces both the thermodynamic and capacitive displacement noise contributions. Second, the ADC noise is reduced because we can use a gain which reflects a lower level of background noise on the Moon. Overall, the noise floor of the instrument is reduced, increasing the proportion of moonquakes that can be detected at any one location.

4. Assessing Detection Rates

The Apollo missions included seismometers which operated at multiple landing sites over periods between 1969 and 1977 (Latham et al. 1971; Nunn et al. 2020). Using the seismic data available from the seismometers deployed by astronauts during these missions (Figure 4), we investigate the number of moonquakes which would be above the detection thresholds for the SSP seismometer. Instruments deployed during the Apollo era detected several types of events, including artificial impacts, meteoroid strikes, shallow and deep moonquakes, and thermal events (Nakamura et al. 1982). Given several years of operations for the Apollo instruments, we have excellent constraints on the lunar seismicity rate over the multi-year catalog (Nakamura et al. 1981). We also have constraints on diurnal variations for thermal events throughout the lunar day/night cycle (Duennebier & Sutton 1974).

Figure 5 shows the spectra for a selection of lunar events recorded by the Apollo mid-period[6] and short-period instruments, ranging from small to very large (large for a natural lunar event). The mid-period instrument had two operational modes: peaked mode (which was most frequently used) and flat mode which recorded to longer periods but was sometimes unstable (Nunn et al. 2020). The plot shows the range (the 10th, 30th, 50th, 70th, and 90th percentiles) of noise spectra, for the mid-period flat and peaked modes, and for the short-period instrument, recorded at Apollo's S14. Numerical glitches, where a single sample has a large error, were common in the Apollo data. We applied a simple deglitching algorithm to the noise traces (removing glitches greater than ±30 digital units from the mean). Inspection of the traces suggests that some small numerical glitches remain, which makes it difficult to estimate the full range of the noise spectra. Based on the 10th percentile of the noise spectra, we show the spectrum of the lowest noise recorded on the Moon (dashed gray line, Figure 5). The spectrum has very low noise amplitudes between 0.3 and 0.5 Hz and higher amplitudes between 1 and 5 Hz. The events follow similar spectra, suggesting that the Moon has a distinctive noise spectrum. For each event, the spectra at 3 Hz are at least one order of magnitude larger than those at 0.3 Hz.

Figure 5 shows a large range in recorded noise spectra, as well as an overlap between the noisier periods and the small

[5] In this paper, g_0 refers to the average acceleration at the surface of the Earth, 9.8 ms^{-2}.

[6] The mid-period instrument was commonly referred to as the long-period (LP) instrument in Apollo-era literature.

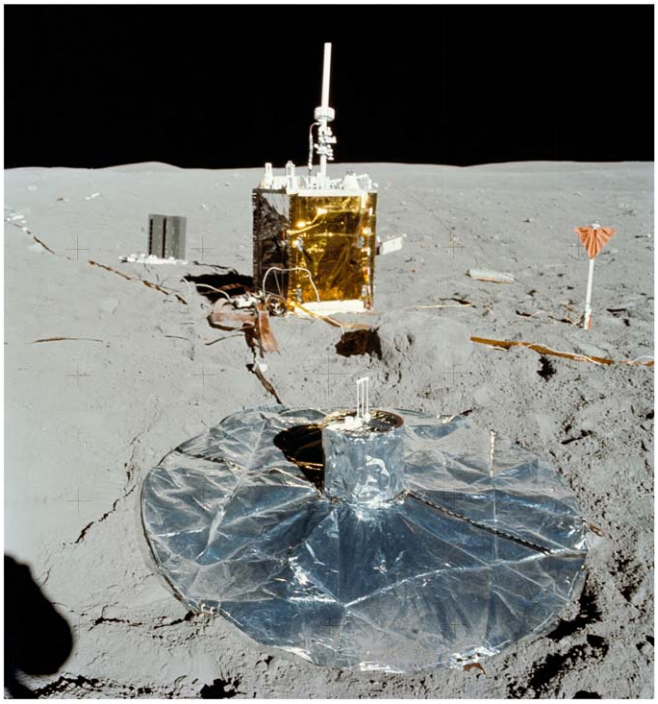

Figure 4. Apollo Lunar Seismic Experiment deployed at the Apollo 16 site. Photo Credit: NASA.

and medium events. Between 0.3 and 0.9 Hz, the small lunar event (dark-green line), which is only just visible on the seismic trace, corresponds to the 50th noise percentile, and the medium event (medium-green line) to the 70th. Figure 5 shows that the predicted noise floor for the SSP instrument is similar to the Apollo instruments between 0.3 and 0.5 Hz, and better than Apollo above 0.5 Hz. Therefore, we expect the micro-seismometer to detect moonquakes at least as well as Apollo.

In addition to the variation between high and low noise at a single site, there was also variation between the different Apollo sites. Figure 6(a) shows the noise spectra at the 10th percentile, and Figure 6(b) at the 90th percentile for each of the Apollo stations. On the mid-period instruments, the lowest recorded noise was at S14 (red line), followed by similar levels for S16 (black line) and S12 (blue line), and with the highest levels for S15 (green line). The short-period instruments show a similar pattern: the lowest noise was observed on S14 (dashed red line), followed by S16 (dashed black line), with the highest noise observed on S15 (dashed green line). For the short-period instrument, S16 has a maxima around 2 Hz, S15 has a maxima around 4.5 Hz, and S12 is smooth at these frequencies. Note that although we show a time when S14 had the lowest noise, S14's vertical component stopped working shortly afterward. Figures 5 and 6 show only the vertical noise, which is generally quieter than the horizontal noise (see Section 9a in plot_seismometer_noise.ipynb in the GitHub repository).

Different numbers of events were detected at the different Apollo stations. The lunar event catalog (Nakamura et al. 1981; also available as a QuakeML file in the electronic supplement of Nunn et al. 2020) contains 3520, 3785, 5785, 6773 events detected at S15, S12, S14, and S16, respectively, between June 1972 (when all the stations were operational) until the end of the mission. Note that the vertical component of S14 was not functioning for much of the period, making it necessary to search for events on the noisier horizontal component, and potentially reducing the number of events detected at S14. The lowest number of events was detected at the noisiest station, which was S15. However, there is no obvious relation between detections and noise at the other stations. Several factors affect detection rates: the sensitivity of the instrument; glitches and problems with the instrument; the background noise at the site; local resonance caused by layering; and the local seismicity. Regolith thickness and the velocity gradients within the subsurface can create seismic resonances in both the event signals and the local noise environment. Nakamura et al. (1975) and Horvath et al. (1980) found variation in regolith thickness and velocity gradients between the different Apollo sites.

Figure 6 also shows examples of typical noise periods for S14 and S15. The Apollo seismic data were digitized on the Moon before being sent to Earth, and the level of digitization was very coarse (see Nunn et al. 2020). The Apollo noise spectra generally cover two to five digitization units (DU) with some periods with amplitudes which are more than $\pm$ 10 from the mean. Figure 6(c) includes brief periods where the digitizer has recorded only a single digital unit (e.g., the flat line in the last three seconds). Finer digitization of the Apollo signals would have improved the fidelity of the smaller signals, giving the signals a clearer onset and a smoother increase in signal amplitude. The traces commonly contain small signals which cannot be resolved, which may potentially be small local events (e.g., Figure 6(f), but probably also Figures 6(d) and 6(e)). These are extremely common, and contaminate most of the one hour records we examined.

We do not see the instrument noise floor at low frequencies for either the short-period or mid-period instruments. The spectra should converge at low frequencies, as they do at high frequencies. This suggests that low frequency noise is contaminating the traces, and making it difficult to accurately remove the instrument response. Coarse digitization of the Apollo seismic records probably contributes to this problem. Alternatively, if the instrument response is not perfectly known, it would be impossible to accurately remove it.

Unsurprisingly, the Moon is generally quieter than the Earth, especially in the region of Earth's secondary microseism (0.1–1 Hz), which is generated by the interaction of oceanic waves and the coast (Darbyshire 1992). Figures 5 and 6 include the Earth's low noise spectrum (Peterson 1993), as well as the lowest noise previously observed on the Moon. Lognonné & Johnson (2015) argued that the recorded low noise represented only the instrument noise floor. Lognonne et al. (2009) estimated a theoretical meteoritic background noise level for the Moon, with peak-to-peak amplitudes smaller than 2×10^{-11} m s^{-2}, which is at least 1000 times lower than the Earth low noise model. Instead, we estimate that the Apollo seismometers recorded reasonably close to the noise environment of the Moon. As described above, there is a wide range of noise amplitudes at each station, which varies with time of lunar day; a difference between stations for both the mid- and short-period instruments; a difference between seismicity rates at the different stations; and the seismic traces usually occupy two to five levels of digitization. Although a seismometer with finer digitization or a lower noise floor would provide some improvements to the fidelity of the signals, and allow for the detection of some smaller signals, we argue that the noise environment of the Moon itself is beginning to limit the number of events that can be seen on the traces. Additionally,

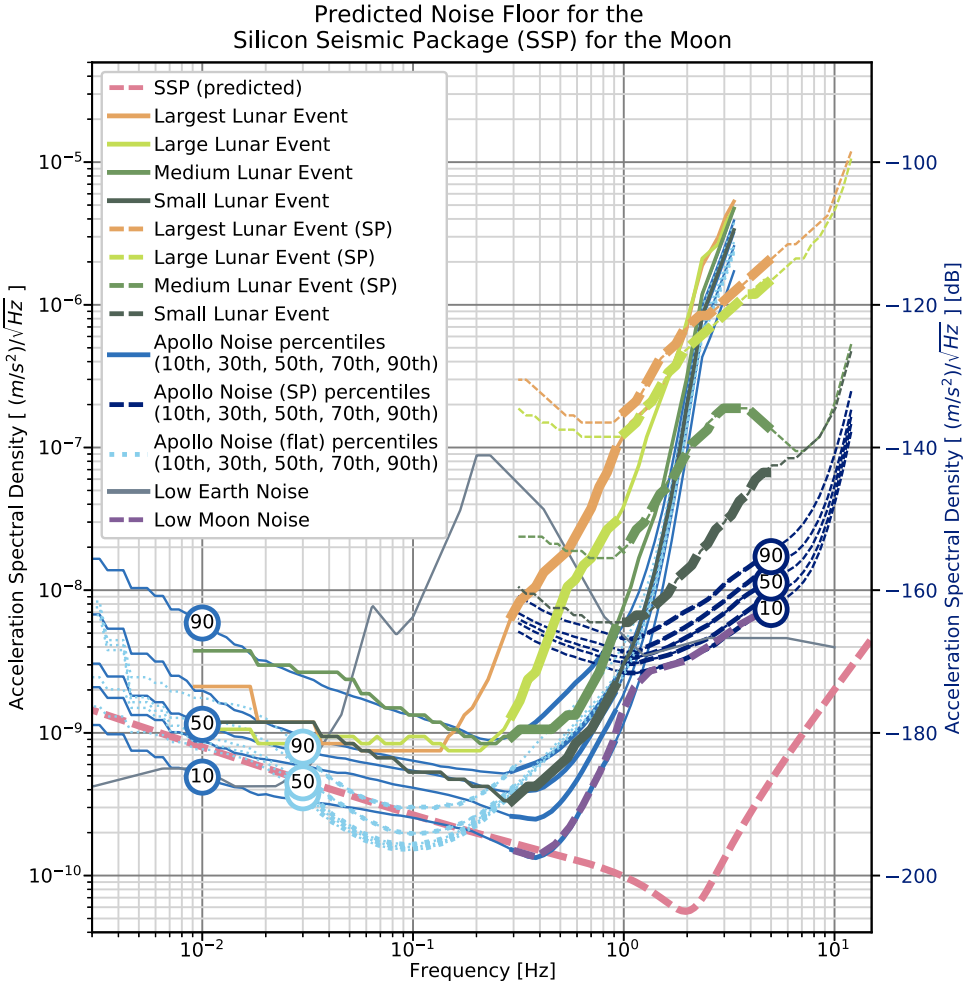

Figure 5. Predicted noise floor for the Silicon Seismic Package (SSP) microseismometer for the Moon (dashed pink line). The plot shows spectra for a small, medium, large, and largest event (dark-green, medium-green, light-green, and orange lines), recorded on Apollo's mid-period, peaked-mode instruments and on the short-period instruments (same colors, dashed lines). The plot also shows noise spectra recorded on the mid-period, peaked-mode, instrument (mid-blue solid lines); S14 short-period instrument (dark-blue dashed lines) and the S12 mid-period instrument in flat mode (light-blue dotted lines). The spectra show the 10th, 30th, 50th, 70th and 90th percentiles (calculated in one hour segments for approximately 28 days). The spectra are most reliable between 0.3 and 0.9 Hz for the mid-period instrument in peaked mode, between 1 and 5 Hz for the short-period instrument and between 3.3 and 33 Hz for the mid-period instrument in flat mode (indicated by thicker lines). For the events, we calculated spectra for ten minutes after the first arrival. All signals were recorded on the vertical component. We applied a simple deglitching algorithm (deleting samples more than 30 digital units from the mean of the trace) to the noise traces, and we selected events which were not affected by numerical glitches. From small to large, the events were: 1973-10-01T04:00 (S16), 1973-07-23T01:14 (S16), 1971-04-17T07:04 (S14), 1973-03-13T08:01 (S12 on the mid-period and S14 on the short-period). Nakamura et al. (1981) classified 1973-07-23T01:14 as a meteoroid impact, and the remaining events as shallow moonquakes. The solid gray line shows the low Seismic Background Noise level for Earth (Peterson 1993), and the dashed purple line shows the lowest noise recorded on the Moon between 0.3 and 5 Hz.

we expect significant differences for each individual future site. As we have only the Apollo signals, it is not possible to say exactly how far below the current low noise spectra for each station the actual lunar noise is.

As event magnitudes are not well known for all events on the Moon, we used the amplitude of the spectra of events to estimate the number of events which could be detected. We selected spectra for events in the catalog Nakamura et al. (1981) for one year (1973), with a relatively clear onset of the initial arrivals, and a signal-to-noise ratio of at least 2.5. Due to the small number of shallow events, we analyzed shallow events for all years and scaled to one year of operation. We calculated spectra for ten minutes after the first arrival. To calculate the cumulative histogram in Figure 7, we used the value of the spectra at 0.45 Hz.

Figure 7 shows that we expect around 74 events above a signal-to-noise ratio of about 2.5, for a single station, and a year of operation (including nighttime operations). The entire catalog (Nakamura et al. (1981) includes over 625 events for the same period, and many of these events are at the very lower limit of detection for the Apollo seismometers. Operation of the seismometer for a single lunar daytime (from soon after dawn to just after dusk) would provide only around three events above a signal-to-noise ratio of 2.5, and a larger number of lower signal-to-noise events. However, because at least about 23 very low-quality events would be expected, it would give a proof of concept for the microseismometer. It would also be an excellent test for the lunar noise environment, and would, therefore, provide a baseline for future missions.

5. Mission Concepts

The ideal case for lunar seismology would be to have several stations recording simultaneously for many years, spaced

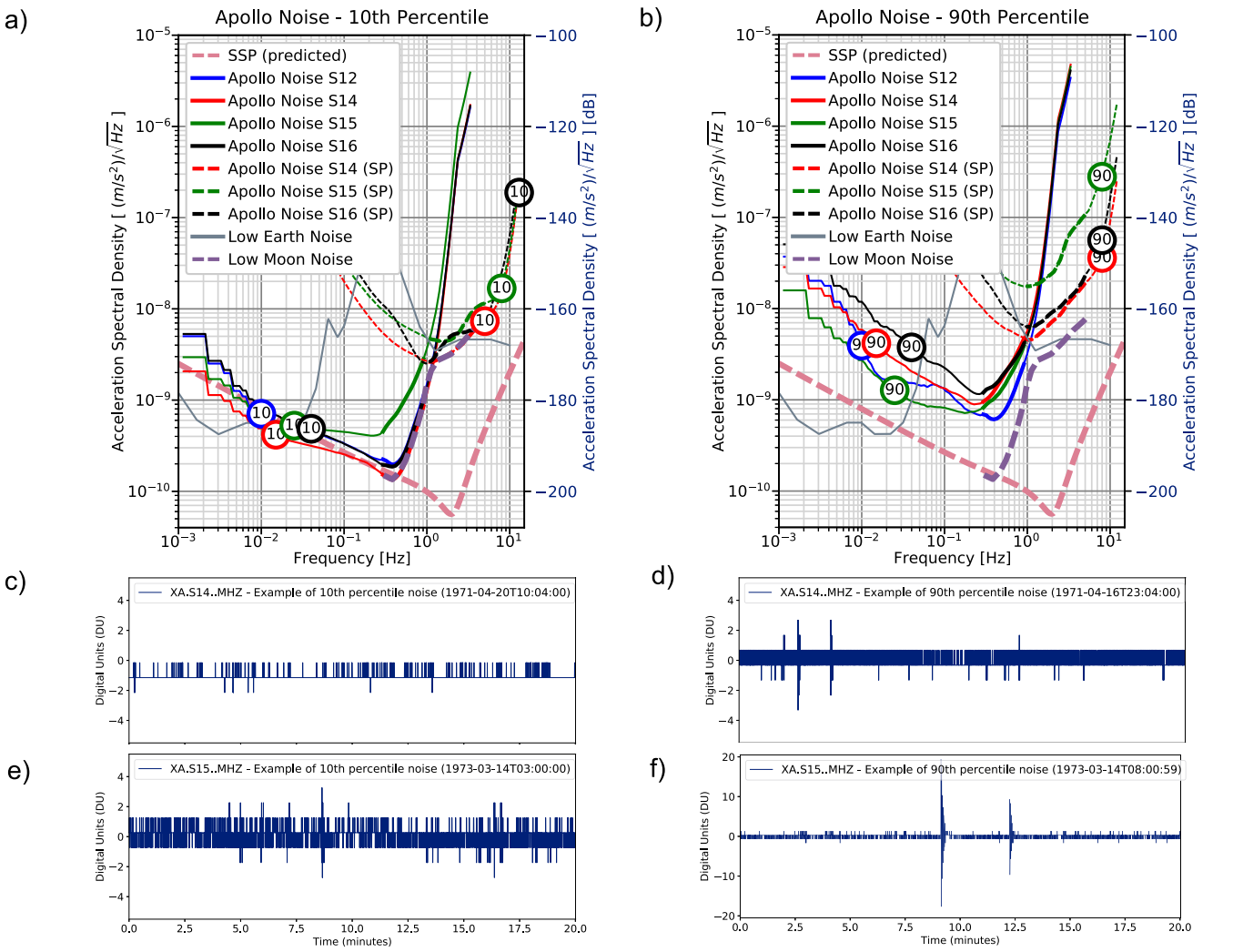

Figure 6. a) Spectra for the 10th percentile of noise and b) for the 90th percentile recorded at the Apollo stations. Spectra are calculated for 28 days in one hour segments. Predicted noise floor for the SSP (dashed pink line), Earth low noise (gray line) and lowest recorded noise on the Moon (dashed purple line) are repeated from Figure 5. The lower subfigures show examples of traces recorded when the noise spectra fit the following percentiles: c) the 10th percentile at S14; d) the 90th percentile at S14; e) the 10th percentile at S15; and f) the 90th percentile at S15. The noise traces show the raw traces (without removing the instrument response). We apply a deglitching algorithm (see Figure 5 caption) to the traces.

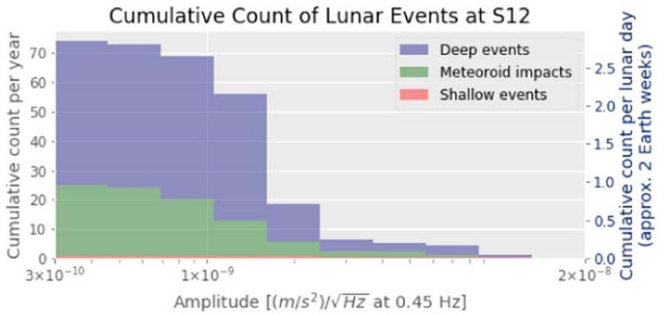

Figure 7. Plot showing a stacked cumulative histogram of lunar events recorded at Apollo 12, with a signal-to-noise ratio above approximately 2.5. The plot shows events classified by Nakamura et al. (1981) as shallow (pink), meteoroid impacts (green) and deep events (purple). We calculated the spectra for each event for ten minutes after the first arrival, and we use its value at 0.45 Hz for the signal amplitude. The left axis shows the expected count for one year and the right axis the time from lunar sunrise to sunset (right axis).

around the Moon. The small size, robustness, and low power consumption of the SSP microseismometer make it a strong candidate for a variety of mission concepts, and also open the possibility of having many stations.

A single instrument, carried on a CLPS mission, would provide a test of the sensors and their night-survivability, and characterize the lunar noise environment. CLPS landers are not currently capable of surviving the lunar night. A short-lived seismic mission (lasting less than 14 Earth days) is difficult to justify. Therefore, we are developing a seismic package with its own power and communications (which could communicate direct to Earth or to a relay satellite). Additionally, there are several advantages for seismic missions to include nighttime operations. First, seismic missions have a greater chance of observing more events as well as larger events the longer they operate. Second, nighttime has lower noise on the Moon, and therefore better signals may be observed. Third, a fully global network requires full-time operation, because it is always

nighttime somewhere on the Moon. A mission which lasted for five years could achieve many science goals, such as estimating the local structure of the subsurface and the thickness of the crust.

More ambitious science goals, such as estimating the state of the core (solid, liquid, or partial melt) and its thickness, would be possible with several instruments operating simultaneously. These instruments could be carried on different CLPS missions. An instrument deployed on the ground (with good ground-coupling or even burial) would probably achieve the best results. Good ground-coupling may potentially reduce noise from the dusty layer near the Moon's surface. However, Panning & Kedar (2019) showed that deck-mounted seismometers record ground motions very well in the absence of wind. Deck-deployment, which would be easier, cheaper, and lower risk has great potential, especially as a ride-share on CLPS. Earth-based monitoring of impact flashes from meteoroids hitting the lunar nearside could be used to provide known seismic sources and locations (reducing the unknowns in the parameterization), allowing for better-calibrated models of the lunar interior. The monitoring program at NASA's Marshall Space Flight Centre observed 300 impacts between 2006 and 2014 (Suggs et al. 2014).

The SSP is a strong candidate for one of the seismic instruments on the LGN. The LGN would have three to four geophysical stations operating simultaneously (Neal et al. 2020b). Several sites are being considered, which would include one on the far-side, and one within the high heat-flow Procellarum KREEP Terrane as well as a lower heat-flow region. In addition to the seismometers, the LGN would carry one or more heat-flow probes, electromagnetic (EM) instrumentation, and laser retroreflectors. The mission would test the lunar magma ocean hypothesis, constrain crustal thickness, measure the temperature of the upper and lower mantle, assess the nature of the lower mantle, and the size, state, structure of the lunar core (Neal et al. 2020a).

NASA's Artemis program would see humans return to the Moon as early as 2024 (NASA 2019). We envision a small, self-sufficient seismic package that could be easily carried and installed by astronauts. We are working on the back-end electronics and the thermal switch to help isolate the instruments from the large diurnal temperature variations on the Moon (Clark et al. 2020).

Finally, we are pursuing a mission concept where clusters of up to eight seismometers would be delivered to several sites around the Moon by penetrators. Penetrators have many potential advantages for planetary targets, including low mass, good ground-coupling, and ease of deployment. Penetrators launched from lunar orbit or ejected before landing would provide a low-cost, low-risk, delivery mechanism for seismometers that can survive a hard landing. Many seismometers could be deployed as a distributed network, covering different regions of the Moon.

Penetrators have been considered as a delivery mechanism for scientific instruments since at least the 1970s (Lorenz 2011). Two penetrators with instrumentation, part of the Deep Space 2 probe, flew on Mars Polar Lander in January 1999 (Smrekar et al. 1999), but the lander and penetrators failed to communicate after landing. The Japan Aerospace Exploration Agency (JAXA) designed a penetrator for LUNAR-A, with seismometers that survived 8000 g impact tests (Yamada et al. 2015). The agency canceled LUNAR-A in 2007, but the penetrator and its seismometer narrowly missed selection for a later mission in 2018.

A large number of penetrators would allow us to tolerate the loss of some penetrators due to the rocky and varied nature of the lunar surface. Two or more penetrators within a cluster would enable us to stack signals, reducing random noise, and increasing the signal-to-noise ratio. There is also an opportunity to reduce non-random noise using the same method. Billions of years of bombardment by meteoroids have left the lunar surface highly fractured. Seismic energy which travels through the fractured layer is scattered, and the resulting seismograms often last for over an hour and have long seismic coda. Stacking the signals could potentially reduce some of the scatter introduced by the near-surface layer, and result in cleaner signals from the core-mantle boundary and other features of interest.

The Deep Space 2 penetrators were designed to impact at speeds between 180 and 200 m s^{-1} (Smrekar et al. 1999). Upon impact they split into two parts: an aftbody that remained on the surface and a forebody designed to penetrate between 0.2 and 0.6 m into the ground (depending on the composition of the regolith). The forebody experienced up to 30,000 g_0, and the aftbody as much as 60,000 g_0 (Smrekar et al. 1999). The microseismometer would be located in the forebody. As described above, Hopf et al. (2010) showed that the sensors can tolerate shocks of 15,000 g_0. Therefore, the sensor tolerance is lower than the projected shock. To ensure that the seismometer can survive the hard shock of an impact landing, further work is required in the following areas: to estimate the upper limit of the shock; to reduce the shock on the forebody; to increase the tolerance of the entire microseismometer; and to test the probe. The tilt tolerance of the seismometer becomes critical, and a mechanism for calculating the orientation of the sensors is required. The expected burial depth would provide excellent ground-coupling, and potentially some thermal shielding of the instruments. Additionally, we will need to test the thermal tolerance of the complete instrument, including any impact on sensitivity or performance.

6. Conclusions

We propose a SSP microseismometer for the Moon. The SSP is robust to high shock and vibration and can operate in a large temperature range, allowing deployment under harsh conditions. The SSP is predicted to have a similar noise floor to the Apollo instruments between 0.3 and 0.5 Hz, and better than Apollo above 0.5 Hz. It is therefore a strong candidate for future lunar missions. The following factors, taken together, suggest that the Apollo instruments may have been recording reasonably close the environmental noise of the Moon: the wide range of noise amplitudes at each station (which varies with time of lunar day); the difference between stations for both the mid- and short-period instruments; the difference between seismicity rates at the different stations; and the observation that the seismic traces usually occupy two to five levels of digitization. The limiting factor for recording smaller moonquakes may be the noise environment of the Moon itself, rather than the noise floor of the instrument. To overcome this potential limitation, we should consider mission architectures with several seismometers deployed at the same site to stack the seismic signals and increase the signal-to-noise ratio.

The SSP is not predicted to perform well at frequencies lower than 0.3 Hz. Therefore, an instrument such as the SEIS-VBB (Lognonné et al. 2019, 2020), currently deployed on

Mars, would be more suitable to detect long-period seismic signals (e.g., Yamada et al. 2013).

The SSP is a candidate for a number of missions, including:

1. CLPS, either as a standalone or integrated into a Lunar Geophysical Package.
2. As a secondary instrument for the LGN.
3. Artemis, within an astronaut-deployed package such as the Lunar Geophysical Package.
4. Deployed in clusters (up to eight instruments) to several locations around the Moon with penetrator missions.

7. GitHub Repository

The accompanying GitHub repository, https://github.com/cerinunn/apollo-shoulders, contains Jupyter notebooks to reproduce the figures in this paper, including the parameters and equations used to produce Figure 3. It also contains example signals and noise from the Moon and Mars, and other background information. An archived version is also available in Zenodo at 10.5281/zenodo.4321769.

C.N. was supported by strategic funds from the Jet Propulsion Laboratory, California Institute of Technology, under a contract with the National Aeronautics and Space Administration.

We thank two anonymous reviewers for their constructive comments. We additionally thank Philippe Lognonné and Yosio Nakamura for their helpful comments which helped improve and clarify the manuscript prior to submission.

We acknowledge NASA, CNES, their partner agencies and Institutions (UKSA, SSO, DLR, JPL, IPGP-CNRS, ETHZ, IC, MPS-MPG) and the flight operations team at JPL, SISMOC, MSDS, IRIS-DMC, and PDS for providing SEED SEIS data (InSight Mars SEIS Data Service 2019). We also acknowledge NASA for seismic data from the Apollo missions, and GEOSCOPE (IPGP) for providing these data.

Software: ObsPy (Beyreuther et al. 2010; Megies et al. 2011).

ORCID iDs

Ceri Nunn https://orcid.org/0000-0001-5647-8001

References

Beyreuther, M., Barsch, R., Krischer, L., et al. 2010, Seismol. Res. Lett., 81, 530
Clark, P. E., Bugby, D., & Cochrane, C. 2020, LPSC, 51, 1526
Darbyshire, J. 1992, PEPI, 73, 282
Duennebier, F., & Sutton, G. H. 1974, JGR, 79, 4351
Gabrielson, T. 1993, ITED, 40, 903
Garcia, R. F., Khan, A., Drilleau, M., et al. 2019, SSRv, 215, 50
Hopf, T., Kumar, S., Karl, W., & Pike, W. 2010, AdSpR, 45, 460
Horvath, P., Latham, G. V., Nakamura, Y., & Dorman, H. J. 1980, JGR, 85, 6572
InSight Mars SEIS Data Service 2019, SEIS raw data, Insight Mission. IPGP, JPL, CNES, ETHZ, ICL, MPS, ISAE-Supaero, LPG, MFSC, https://doi.org/10.18715/SEIS.INSIGHT.XB_2016
Latham, G., Ewing, M., Dorman, J., et al. 1971, Sci, 174, 687
Lognonné, P., Banerdt, W. B., Giardini, D., et al. 2019, SSRv, 215, 12
Lognonné, P., Banerdt, W. B., Pike, W. T., et al. 2020, NatGe, 13, 213
Lognonné, P., & Johnson, C. 2015, in Treatise on Geophysics, ed. G. Schubert (Oxford: Elsevier), 65
Lognonne, P., Le Feuvre, M., Johnson, C. L., & Weber, R. C. 2009, JGRE, 114, E12003
Lorenz, R. D. 2011, AdSpR, 48, 403
Megies, T., Beyreuther, M., Barsch, R., Krischer, L., & Wassermann, J. 2011, AnGeo, 54, 47
Nakamura, Y., Dorman, J., Duennebier, F., Lammlein, D., & Latham, G. 1975, The Moon, 13, 57
Nakamura, Y., Latham, G. V., & Dorman, H. J. 1982, JGR, 87, A117
Nakamura, Y., Latham, G. V., Dorman, H. J., & Harris, J. E. 1981, Passive Seismic Experiment Long-Period Event Catalog, Final Version, Galveston Geophysics Laboratory of the University of Texas at Austin, Marine Science Institute
NASA 2019, NASA Selects 12 New Lunar Science, Technology Investigations, http://www.nasa.gov/press-release/nasa-selects-12-new-lunar-science-technology-investigations
Neal, C., Weber, R. C., Amato, J. M., et al. 2020a, The Lunar Geophysical Network (Planetary Missions Concept Studies Report), Tech. Rep. Submitted in Response to: NNH18ZDA001N-PMCS, https://science.nasa.gov/files/science-red/s3fs-public/atoms/files/Lunar%20Geophysical%20Network.pdf
Neal, C., Weber, R. C., Banerdt, W. B., et al. 2020b, 51st Lunar Planetary Science Conference, https://www.hou.usra.edu/meetings/lpsc2020/pdf/2355.pdf
Nunn, C., Garcia, R. F., Nakamura, Y., et al. 2020, SSRv, 216, 89
Panning, M. P., & Kedar, S. 2019, Icar, 317, 373
Peterson, J. 1993, US Geological Survey, Open-file Report, 93, 322
Pike, W. T., Calcutt, S., Standley, I., et al. 2016a, in 25-European Lunar Symposium 2016-NASA (Amsterdam: Royal Netherlands Academy of Arts and Sciences), 27, https://els2016.arc.nasa.gov/downloads/ELS_2016_Abstract_Booklet_v2.pdf
Pike, W. T., Calcutt, S., Standley, I., et al. 2016b, LPSC, 47, 2081
Pike, W. T., Standley, I. M., & Calcutt, S. 2013, 2013 Transducers, Eurosensors XXVII: The 17th Int. Conf. Solid-State Sensors, Actuators and Microsystems (Barcelona,: IEEE), 622
Pike, W. T., Standley, I. M., Calcutt, S., & Mukherjee, A. G. 2018, in 2018 IEEE Micro Electro Mechanical Systems (MEMS) (Piscataway, NJ: IEEE)
Richardson, D. 2019, NASA Selects Experiments to Fly Aboard Commercial Lunar Landers, https://www.spaceflightinsider.com/organizations/nasa/nasa-selects-experiments-to-fly-aboard-commercial-lunar-landers/
Smrekar, S., Catling, D., Lorenz, R., et al. 1999, JGR, 104, 27013
Suggs, R., Moser, D., Cooke, W., & Suggs, R. 2014, Icar, 238, 23
Yamada, R., Garcia, R. F., Lognonné, P., et al. 2013, P&SS, 81, 18
Yamada, R., Nébut, T., Shiraishi, H., et al. 2015, AdSpR, 56, 341